

Nucleon form factors with light Wilson quarks

**Jeremy Green^{*,a†}, Michael Engelhardt,^b Stefan Krieg,^{cd} Stefan Meinel,^a
John Negele,^a Andrew Pochinsky^a and Sergey Syritsyn^e**

^a*Center for Theoretical Physics, Massachusetts Institute of Technology,
Cambridge, Massachusetts 02139, USA*

^b*Department of Physics, New Mexico State University, Las Cruces, New Mexico 88003, USA*

^c*Bergische Universität Wuppertal, D-42119 Wuppertal, Germany*

^d*IAS, Jülich Supercomputing Centre, Forschungszentrum Jülich, D-52425 Jülich, Germany*

^e*Lawrence Berkeley National Laboratory, Berkeley, California 94720, USA*

E-mail: green@kph.uni-mainz.de, engel@nmsu.edu,
s.krieg@fz-juelich.de, smeinel@mit.edu, negele@mit.edu, avp@mit.edu,
ssyritsyn@lbl.gov

We present nucleon observables — primarily isovector vector form factors — from calculations using $2 + 1$ flavors of Wilson quarks. One ensemble is used for a dedicated high-precision study of excited-state effects using five source-sink separations between 0.7 and 1.6 fm. We also present results from a larger set of calculations that include an ensemble with pion mass 149 MeV and box size 5.6 fm, which nearly eliminates the uncertainty associated with extrapolation to the physical pion mass. The results show agreement with experiment for the vector form factors, which occurs only when excited-state contributions are reduced. Finally, we show results from a subset of ensembles that have pion mass 254 MeV with varying temporal and spatial box sizes, which we use for a controlled study of finite-volume effects and a test of the “ $m_\pi L = 4$ ” rule of thumb.

*31st International Symposium on Lattice Field Theory LATTICE 2013
July 29 – August 3, 2013
Mainz, Germany*

^{*}Speaker.

[†]Current affiliation: *Institut für Kernphysik, Johannes Gutenberg-Universität Mainz, D-55099 Mainz, Germany*

1. Introduction

The isovector Dirac and Pauli form factors are defined via nucleon matrix elements of the vector current:

$$\langle N(p') | \bar{\psi} \gamma^\mu \tau^a \psi | N(p) \rangle = \bar{u}(p') \left(\gamma^\mu F_1^v(Q^2) + \frac{i \sigma^{\mu\nu} q_\nu}{2m} F_2^v(Q^2) \right) \tau^a u(p), \quad (1.1)$$

where $\psi^T = (u, d)$, $q = p' - p$, and $Q^2 = -q^2$. For connecting with experiment, this means that

$$F_{1,2}^v = F_{1,2}^p - F_{1,2}^n, \quad (1.2)$$

where $F_{1,2}^{p,n}$ are form factors of the electromagnetic current in a proton and in a neutron. Near zero momentum transfer, these contain the isovector Dirac and Pauli radii and anomalous magnetic moment:

$$F_1^v(Q^2) = 1 - \frac{1}{6} (r_1^v)^2 Q^2 + \mathcal{O}(Q^4) \quad (1.3)$$

$$F_2^v(Q^2) = \kappa^v \left(1 - \frac{1}{6} (r_2^v)^2 Q^2 + \mathcal{O}(Q^4) \right). \quad (1.4)$$

In recent years there has been increased attention paid to the problem of excited-state contamination in lattice QCD calculations of nucleon structure observables. These arise when the Euclidean time separations between the nucleon source and the vector current, and between the vector current and the nucleon sink, are too small to effectively filter out other states with the same quantum numbers as the ground-state nucleon. In Sec. 2, we report results from a high-precision study of excited-state effects using calculations with multiple source-sink separations, which allow for testing different methods for computing matrix elements.

We also report results from a separate set of calculations using eleven lattice ensembles with a range of pion masses and lattice volumes. We show in Sec. 3 that good agreement with experiment for the isovector vector form factors is achieved only when excited states are under reasonable control and the pion mass is near the physical point. In Sec. 4, we describe the results of a controlled study of finite-volume effects using four ensembles with $m_\pi = 254$ MeV.

2. High-precision study of excited-state effects

For studying excited-state effects, we use a single ensemble generated by USQCD with $2 + 1$ flavors of Wilson-clover fermions coupled to gauge fields smeared with one level of stout smearing, as was used for $N_f = 3$ ensembles in Ref. [1]. This ensemble has lattice volume $32^3 \times 96$, lattice spacing $a \approx 0.11$ fm, and pion mass $m_\pi \approx 317$ MeV. On it, we compute nucleon observables using five source-sink separations $T/a \in \{6, 8, 10, 12, 14\}$, covering a range between 0.7 and 1.6 fm. High precision is achieved by performing 24672 measurements on 1028 gauge configurations.

We use three different methods for computing matrix elements from two-point and three-point correlators:

1. The traditional *ratio-plateau* method. For each source-sink separation, averaging over a fixed number of points at the center of each plateau yields a result with excited-state contributions

asymptotically falling off as $e^{-\Delta E_{10}^{\min} T/2}$, where $\Delta E_{10}^{\min} = \min\{\Delta E_{10}(\vec{p}), \Delta E_{10}(\vec{p}')\}$ and the latter are the energy gaps between the ground state and the first excited state at the source and at the sink.

2. The *generalized pencil-of-function*, or GPoF, method [2]. This is based on the recognition that the time-displaced nucleon interpolating operator $N^\tau(t) \equiv N(t + \tau)$ is linearly independent from $N(t)$. Therefore, by combining three-point correlators with three equally-spaced source-sink separations, we can use the variational method [3, 4] to find linear combinations of N and N^τ that asymptotically eliminate the lowest-lying excited state. Applying the ratio-plateau method to the result yields the ground-state matrix element with excited-state contributions that behave like $e^{-\Delta E_{20}^{\min} T/2}$.
3. The *summation* method involves using the ratio method, summing over the operator-insertion time, and finding the dependence of the resulting sums on the source-sink separation. This requires at least two source-sink separations, but asymptotically reduces the excited-state errors to $Te^{-\Delta E_{10}^{\min} T}$ [5, 6].

With the data collected on this ensemble, the dependence on source-sink separation of each of these methods can be probed: the five source-sink separations yield five different ratio-method results; using GPoF with $\tau = 2a$ makes use of three adjacent source-sink separations, which can be the lowest, middle, or largest three to yield three different results; and taking the difference between sums at adjacent source-sink separations yields four different summation-method results. The resulting Dirac and Pauli form factors computed using these methods are shown in Fig. 1.

The effect of excited-state contamination can be clearly seen in the ratio-method data at low source-sink separations. The value of $F_1(Q^2)$ tends to decrease as excited states are removed by increasing the source-sink separation, and this effect grows stronger at larger Q^2 . The result is that the value of the Dirac radius, given by the slope of $F_1(Q^2)$ at $Q^2 = 0$, tends to increase as excited-state effects are removed.

At low Q^2 , the value of $F_2(Q^2)$ shows a strong increase with the source-sink separation; this effect decreases at larger Q^2 , and between 0.5 and 0.7 GeV^2 it appears to change sign. This means that the slope and the intercept, extrapolated to $Q^2 = 0$, will both grow as excited-state effects are removed, causing the computed values of the magnetic moment and Pauli radius to increase.

For the Dirac form factor, the ratio method appears to stabilize at a plateau by the third or fourth source-sink separation, i.e., around 1.1 to 1.3 fm. The ratio data for the Pauli factor at low Q^2 generally don't appear to be approaching a plateau, although it is possible that the apparent accelerating growth with the source-sink separation may simply be a random fluctuation of correlated data; comparing momentum transfer #4 with the adjacent two suggests that this may be the case.

The GPoF method produces results that are quite similar to what is obtained from the ratio method using the largest of the three source-sink separations used for GPoF, although with slightly larger errors.

The power of the summation method for eliminating excited-state contamination can be seen by considering the smallest two source-sink separations. Using the ratio method, this produces the first two ratio points in the plots, which suffer from significant excited-state effects. However, the same data can be combined to produce the first set of summation points, which are generally

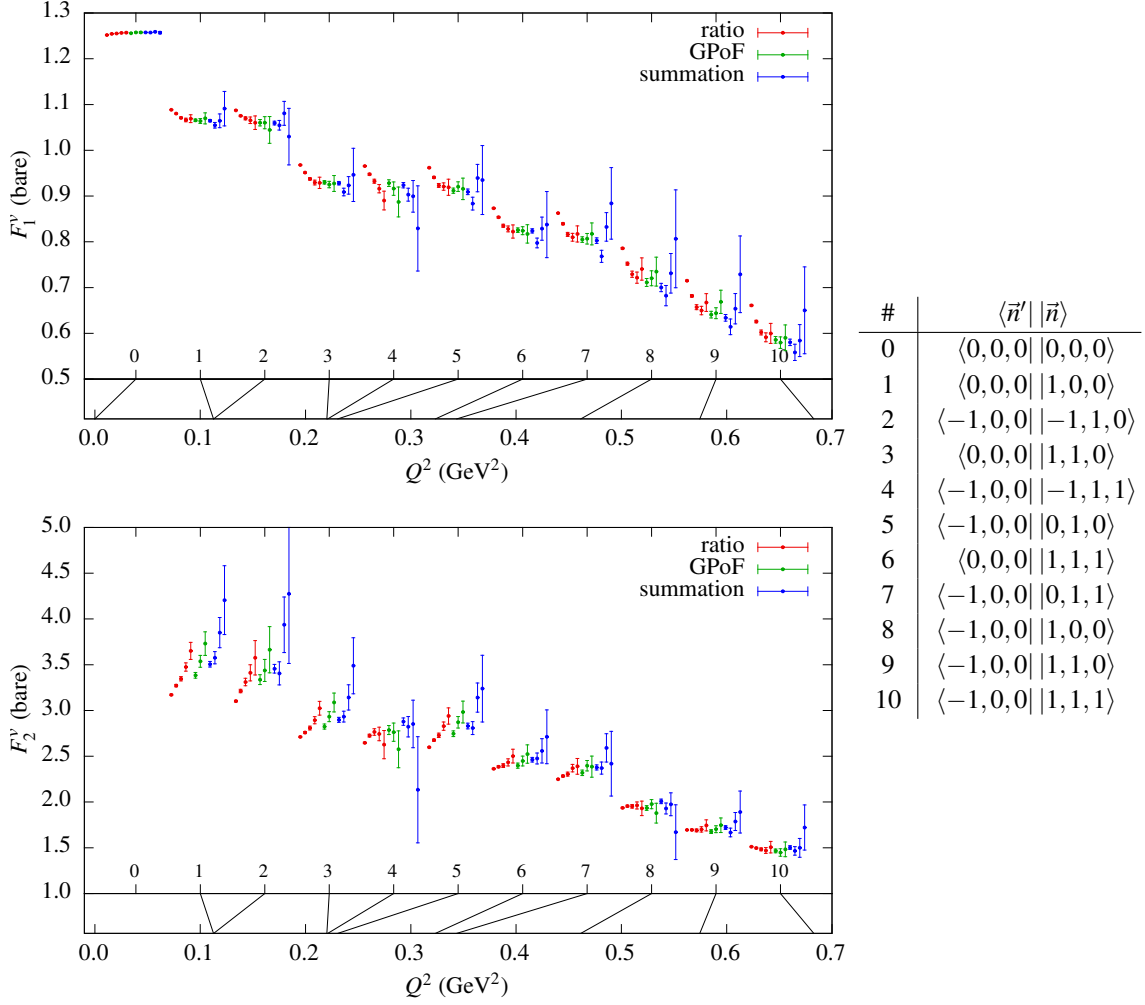


Figure 1: Isovector Dirac and Pauli form factors $F_1^v(Q^2)$ and $F_2^v(Q^2)$ on the USQCD ensemble, computed using the ratio, GPoF, and summation methods. Each method is shown with multiple points at each Q^2 , corresponding to different source-sink separations increasing from left to right. The table lists representative source and sink momenta ($\vec{p} = \frac{2\pi}{L_s} \vec{n}$ and $\vec{p}' = \frac{2\pi}{L_s} \vec{n}'$, respectively) for each momentum transfer Q^2 .

compatible with the plateau ultimately obtained using the ratio method (for F_1) or with the fourth ratio-method point (for F_2). On the other hand, the summation method produces rather large statistical errors, so it is still not clear as to whether the summation method is generally superior to simply using the ratio method at larger source-sink separations.

3. Isovector vector form factors near the physical pion mass

Our larger set of calculations uses the action developed by the BMW collaboration, with $2 + 1$ flavors of Wilson-clover fermions coupled to gauge fields smeared with two levels of HEX smearing [7]. We use mostly “coarse” ensembles with $a = 0.116$ fm and pion masses ranging from the near-physical 149 MeV to 356 MeV, with spatial box sizes that mostly satisfy $m_\pi L_s \gtrsim 4$.

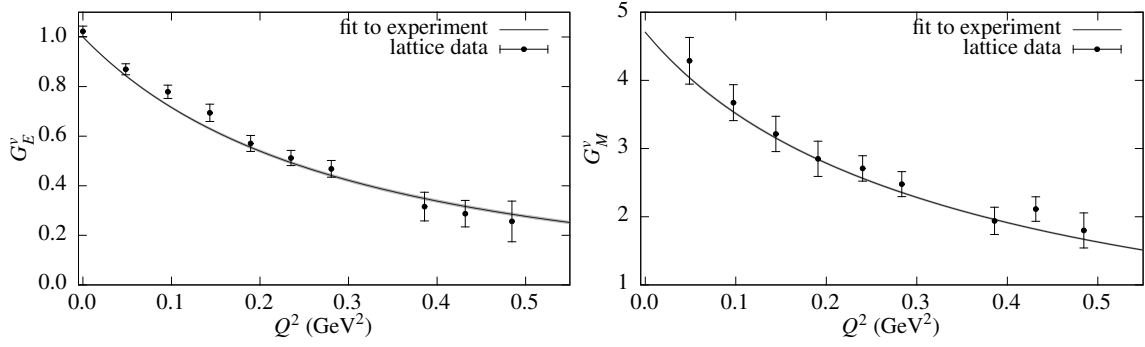


Figure 2: Isovector electric and magnetic form factors, computed on the $m_\pi = 149$ MeV ensemble using the summation method (data at nearby Q^2 are binned for clarity). The curves are from the fit to experiment in Ref. [9].

On each ensemble, we compute three-point correlators using three source-sink separations that are close to the middle three used for the high-precision study in the previous section. Because the data are noisier than in the previous section, we use the summation method in just one way, fitting a line to the sums for the three source-sink separations.

With these ensembles, we performed dipole fits in the range $0 \leq Q^2 < 0.5$ GeV² to determine the Dirac and Pauli radii and the anomalous magnetic moment. Using the summation method and extrapolating these quantities to the physical pion mass produced agreement with experiment [8], and their values on the ensemble with $m_\pi = 149$ MeV and $L_s = 5.6$ fm were also close to the experimental values.

To avoid the complications involved in determining behavior at $Q^2 = 0$, it is interesting to compare the form factors themselves with experiment. To that end, we plot the Sachs form factors,

$$G_E^v(Q^2) = F_1^v(Q^2) - \frac{Q^2}{2m_N} F_2^v(Q^2) \quad (3.1)$$

$$G_M^v(Q^2) = F_1^v(Q^2) + F_2^v(Q^2), \quad (3.2)$$

from the $m_\pi = 149$ MeV ensemble together with experimental curves that include experimental uncertainties [9], in Fig. 2. The lattice data are consistent with experiment ($p = 0.64$ for G_E and $p = 0.81$ for G_M), but this is only achieved with both reasonable control over excited states and a near-physical pion mass. If either of these conditions is not satisfied, then the agreement fails; for example, using the ratio method with $T = 1.16$ fm or using an ensemble with $m_\pi = 254$ MeV yields $p < 10^{-3}$.

4. Controlled study of finite-volume effects

A particular subset of the ensembles used for the calculations described in the previous section allows for a controlled study of finite-volume effects. This consists of four ensembles with $m_\pi = 254$ MeV that differ only in their space and time extents: with $a = 0.116$ fm, these are $24^3 \times 24$, $24^3 \times 48$, $32^3 \times 24$, and $32^3 \times 48$. We look for the volume dependence of a given observable by fitting

$$A + Be^{-m_\pi L_s} + Ce^{-m_\pi L_t} \quad (4.1)$$

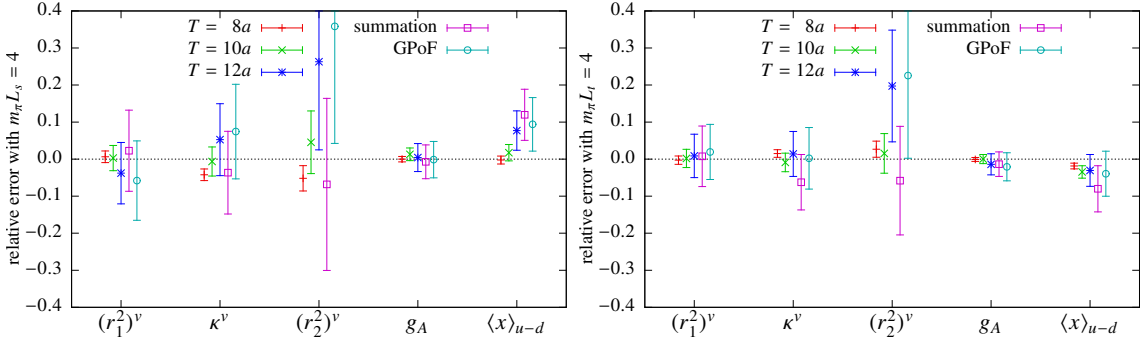


Figure 3: Relative finite-volume errors from ensembles with $m_\pi = 254$ MeV, interpolated to $m_\pi L_s = 4$ and $m_\pi L_t = 4$. In terms of the fit parameters in Eq. 4.1, the plotted data are $e^{-4}B/A$ and $e^{-4}C/A$.

to the four data points. We then use this for interpolating to test the “ $m_\pi L = 4$ ” rule of thumb and determine the relative error caused by $m_\pi L_s = 4$ and $m_\pi L_t = 4$ via $e^{-4}B/A$ and $e^{-4}C/A$, respectively.

Using the summation-method results, we find that finite-volume errors are consistent with zero for $(r_1^2)^\nu$, $(r_2^2)^\nu$, and κ^ν , although the statistical uncertainties are moderately large: for $e^{-4}B/A$, they are roughly 0.1 for $(r_1^2)^\nu$ and κ^ν , and 0.2 for $(r_2^2)^\nu$; the corresponding statistical uncertainties for $e^{-4}C/A$ are slightly smaller.

Reduced statistical uncertainties can be obtained by using the ratio method, although there is the possibility that volume dependence could be caused by volume-dependent excited-state effects (such as those from multiparticle states), rather than a finite-volume effect in the ground state. For $(r_1^2)^\nu$, the ratio method at $T = 0.93$ fm still shows no sign of finite-volume effects, and the statistical uncertainty at $m_\pi L = 4$ is reduced to 0.02. On the other hand, the same method indicates that κ^ν and $(r_2^2)^\nu$ suffer from a -5% shift at $m_\pi L_s = 4$ and a similar shift in the opposite direction at $m_\pi L_t = 4$.

These results are summarized in Fig. 3, where we also show the axial charge g_A and the isovector average quark momentum fraction $\langle x \rangle_{u-d}$. The former shows finite-volume effects consistent with zero and (at the one-sigma level) smaller than those observed in Ref. [10]; using the shortest source-sink separation suggests that such effects are smaller than 1% when $m_\pi L = 4$. On the other hand, the latter does show signs of finite-volume effects, with shifts in opposite directions caused by finite spatial and temporal extents.

5. Conclusions

It has become clear that the use of multiple source-sink separations for identifying and controlling the presence of excited-state contamination is essential for a realistic calculation of nucleon structure observables using lattice QCD. Applying the summation method on an ensemble with a near-physical pion mass, we calculated isovector electric and magnetic form factors that are consistent with experiment.

Using a fully-controlled study of finite-volume effects at $m_\pi = 254$ MeV, we found no such effects for the isovector Dirac radius or the axial charge, at the presently-available level of precision, and an indication of some possible non-negligible effects for the isovector Pauli radius, anomalous magnetic moment, and quark momentum fraction.

Acknowledgments

We thank Zoltan Fodor for useful discussions and the Budapest-Marseille-Wuppertal collaboration for making some of their configurations available to us. This research used resources of the Argonne Leadership Computing Facility at Argonne National Laboratory, which is supported by the Office of Science of the U.S. Department of Energy under contract #DE-AC02-06CH11357, resources at Forschungszentrum Jülich, and facilities of the USQCD Collaboration, which are funded by the Office of Science of the U.S. Department of Energy.

During this research JG, SK, SM, JN, AP and SS were supported in part by the U.S. Department of Energy Office of Nuclear Physics under grant #DE-FG02-94ER40818, ME was supported in part by DOE grant #DE-FG02-96ER40965, SS was supported in part by DOE contract #DE-AC02-05CH11231, SK was supported in part by Deutsche Forschungsgemeinschaft through grant SFB-TRR 55, and JG was supported in part by the PRISMA Cluster of Excellence at the University of Mainz.

Calculations were performed with Qlua [11], except for the propagator solves for the high-precision study of excited-state effects, which were done with the Chroma software suite [12], using QUDA [13] with multi-GPU support [14].

References

- [1] S. R. Beane, E. Chang, S. D. Cohen, W. Detmold, H. W. Lin *et al.*, *Phys. Rev. D* **87** (2013) 034506 [[1206.5219](#)].
- [2] C. Aubin and K. Orginos, *AIP Conf. Proc.* **1374** (2011) 621–624 [[1010.0202](#)].
- [3] M. Lüscher and U. Wolff, *Nucl. Phys. B* **339** (1990) 222–252.
- [4] B. Blossier, M. Della Morte, G. von Hippel, T. Mendes and R. Sommer, *JHEP* **0904** (2009) 094 [[0902.1265](#)].
- [5] S. Capitani, B. Knippschild, M. Della Morte and H. Wittig, *PoS LATTICE2010* (2010) 147 [[1011.1358](#)].
- [6] J. Bulava, M. A. Donnellan and R. Sommer, *PoS LATTICE2010* (2010) 303 [[1011.4393](#)].
- [7] S. Dürr, Z. Fodor, C. Hoelbling, S. Katz, S. Krieg *et al.*, *JHEP* **1108** (2011) 148 [[1011.2711](#)].
- [8] J. R. Green, M. Engelhardt, S. Krieg, J. W. Negele, A. V. Pochinsky *et al.*, [1209.1687](#).
- [9] W. M. Alberico, S. M. Bilenky, C. Giunti and K. M. Graczyk, *Phys. Rev. C* **79** (2009) 065204 [[0812.3539](#)].
- [10] T. Yamazaki, Y. Aoki, T. Blum, H. W. Lin, M. F. Lin *et al.*, *Phys. Rev. Lett.* **100** (2008) 171602 [[0801.4016](#)].
- [11] A. Pochinsky, “Qlua.” <https://usqcd.lns.mit.edu/qlua>.
- [12] R. G. Edwards and B. Joó, *Nucl. Phys. Proc. Suppl.* **140** (2005) 832 [[hep-lat/0409003](#)].
- [13] M. Clark, R. Babich, K. Barros, R. Brower and C. Rebbi, *Comput. Phys. Commun.* **181** (2010) 1517–1528 [[0911.3191](#)].
- [14] R. Babich, M. A. Clark, B. Joó, G. Shi, R. C. Brower and S. Gottlieb, in *Proceedings of 2011 International Conference for High Performance Computing, Networking, Storage and Analysis, SC '11*, (New York, NY, USA), pp. 70:1–70:11, ACM, 2011. [1109.2935](#).